Available on the CERN CDS information server **CMS PAS SMP-16-009**

CMS Physics Analysis Summary

Contact: cms-pag-conveners-smp@cern.ch 2016/08/04

Measurement of the differential Drell-Yan cross section in proton-proton collisions at $\sqrt{s} = 13$ TeV

The CMS Collaboration

Abstract

We present measurement of the differential Drell-Yan cross section $d\sigma/dm$. The analysis is based on the full 2015 dataset, corresponding to an integrated luminosity of 2.8 fb^{-1} of proton-proton collision data collected by the CMS detector. The cross section measurement is reported in the dimuon invariant mass range from 15 to 3000 GeV. The results are corrected to the full phase space and the effects of final state radiation are also taken into account. The data are compared to perturbative QCD predictions. The results are found to be in good agreement with the standard model predictions.

1 Introduction

The Drell–Yan (DY) production of lepton pair at the CERN LHC occurs via s-channel exchange of Z/γ^* bosons. Theoretical predictions of the differential cross section in the standard model (SM) are available and well established up to the next-to-next-to-leading order (NNLO) in quantum chromodynamics (QCD) [1–4]. Precise measurements of the differential cross section provide tests of perturbative QCD, validate the theoretical predictions of higher-order corrections, and constrain the parton distribution functions (PDFs). In addition, DY lepton-pair production is a major source of background not only for rare SM processes but also searches for physics beyond SM [5]. The differential ($d\sigma/dm$) and double-differential ($d\sigma/dmd|y|$) cross sections, where m is the dilepton invariant mass and $|y|$ is the absolute value of the dilepton rapidity, were previously measured by ATLAS [6, 7] and CMS [8–10] Collaborations at $\sqrt{s}$ of 7 and 8 TeV. This Physics Analysis Summary presents measurements of the DY differential cross section $d\sigma/dm$ in the dimuon channel at $\sqrt{s} = 13$ TeV with the full 2015 dataset corresponding to an integrated luminosity of up to 2.8 fb^{-1}.

A counting experiment is performed in this analysis and the measured differential cross section is determined using the following formula:

$$\sigma = \frac{N_u}{A \cdot \varepsilon \cdot \rho \cdot \mathcal{L}_{int}}, \tag{1}$$

where N_u denotes the signal yield after subtracting backgrounds obtained using an unfolding technique to correct for the effect of the migration due to the detector resolution and the final-state QED radiation (FSR) effect. In the formula, A and ε are the acceptance and efficiency for signal events and are obtained from MC simulation. In addition, ρ is the scale factor to account for the difference in the efficiency between data and MC. The $\mathcal{L}_{int}$ is the integrated luminosity of 2015 dataset. The FSR effect is also corrected using the unfolding technique.

This note is organised as follows: in section 2 the CMS detector is described. Section 3 describes the dataset and Monte Carlo (MC) samples used in this analysis. Event selection and background estimation are discussed in section 4 and 5 respectively. All correction procedures are discussed in section 6. Section 6.1 presents the unfolding technique to correct the detector resolution. Section 6.2 and 6.3 provide the acceptance and efficiency corrections as well as the scale factor for the efficiency. FSR effects corrected by the unfolding technique are described in section 6.4. In section 7 and 8, the systematic uncertainty of the measurement and result are presented. Section 9 gives a summary of this measurement.

2 The CMS Detector

The central feature of the CMS apparatus is a superconducting solenoid of 6 m internal diameter, providing a magnetic field of 3.8 T. Within the superconducting solenoid volume are a silicon pixel and strip tracker, a lead tungstate crystal electromagnetic calorimeter (ECAL), and a brass and scintillator hadron calorimeter (HCAL), each composed of a barrel and two endcap sections. Muons are measured in gas-ionization detectors embedded in the steel flux-return yoke outside the solenoid. Extensive forward calorimetry complements the coverage provided by the barrel and endcap detectors.

The electromagnetic calorimeter consists of 75 848 lead tungstate crystals which provide coverage in pseudorapidity $|\eta| < 1.479$ in a barrel region (EB) and $1.479 < |\eta| < 3.0$ in two endcap regions (EE). A preshower detector consisting of two planes of silicon sensors interleaved with

a total of $3X_0$ of lead is located in front of the EE. The electron momentum is estimated by combining the energy measurement in the ECAL with the momentum measurement in the tracker. The momentum resolution for electrons with $p_T \approx 45$ GeV from $Z \to ee$ decays ranges from 1.7% for nonshowering electrons in the barrel region to 4.5% for showering electrons in the endcaps [11].

Muons are measured in the pseudorapidity range $|\eta| < 2.4$, with detection planes made using three technologies: drift tubes, cathode strip chambers, and resistive plate chambers. Matching muons to tracks measured in the silicon tracker results in a relative transverse momentum resolution for muons with $20 < p_T < 100$ GeV of 1.3–2.0% in the barrel and better than 6% in the endcaps, The p_T resolution in the barrel is better than 10% for muons with p_T up to 1 TeV [12]. A more detailed description of the CMS detector, together with a definition of the coordinate system used and the relevant kinematic variables, can be found in Ref. [13].

The first level (L1) of the CMS trigger system, composed of custom hardware processors, uses information from the calorimeters and muon detectors to select the most interesting events in a fixed time interval of less than 4 μs. The high-level trigger (HLT) processor farm further decreases the event rate from around 100 kHz to less than 1 kHz, before data storage.

3 Datasets

The CMS 2015 data samples are used in the analysis, corresponding to an integrated luminosity of 2.8 fb^{-1}. The data are collected with inclusive single lepton triggers. The events are triggered by the presence of at least one muon candidate with $p_T > 20$ GeV and $|\eta| < 2.4$, with the combinations of two different isolation requirements.

Various MC samples are used to simulate the DY signal and backgrounds processes. The MADGRAPH5_AMC@NLO event generator [14] provides signal events using the NNPDF 3.0 [15, 16] PDF. The FxFx technique is used to merge jet multiplicities [17]. Top pair and single top productions are generated using POWHEG based generators [18–21]. Diboson backgrounds are produced by PYTHIA8. The PYTHIA8 [22] generator is used for the parton shower and hadronization with the `TuneCUETP8M1` [23] tune. Detector response in the MC samples is simulated using a detailed description of the CMS detector, based on GEANT4 [24]. Minimum bias events are superimposed on the simulated events to emulate the effects of pileup (multiple interactions per bunch crossing) with an average number of 20 per beam crossing and all MC samples are reweighted to provide the correct distribution of the number of pp interactions per bunch crossing as measured in the data.

4 Event Selection

The offline reconstruction of muons starts with the reconstruction of muon candidates in muon detectors. Candidates from muon detectors are matched to the tracks from the inner tracking systems. Each reconstructed offline muon is required to pass the muon identification criteria that are based on the number hits found in the tracker, the response of the muon detectors, and a set of matching criteria between the muon track parameters as measured by the inner tracker and muon detectors. To reject cosmic-ray muons that can appear as back-to-back dimuons, a small impact parameter with respect to the centre of the interaction region is required. Additionally the opening angle between two muons is required to differ from π by more than 5 mrad. In order to suppress nonprompt muons coming from pion and kaon decays mostly, both muons should be isolated from tracks within a cone of size $\Delta R = 0.3$ ($\Delta R = \sqrt{(\Delta\eta)^2 + (\Delta\phi)^2}$)

and a requirement on a common vertex for the two muons is imposed. More details on muon reconstruction and identification used in this analysis are described in [12, 25].

The leading muon in the event is required to have $p_T > 22$ GeV and subleading muon $p_T > 10$ GeV in order to maximise the acceptance in this analysis. All muons should be within the acceptance of the muon system ($|\eta| < 2.4$). The two muons are required to have opposite-charge and the pair with the smallest χ^2 for the dimuon vertex is selected if there is more than one muon pair in same event. At least one of the two muons selected in each event should match the trigger object.

The measurements are performed in 43 dilepton invariant mass bins. The edge of mass bins is identical as previous measurements [10]. The highest mass event observed in the dataset is 2.3 TeV and therefore the highest mass bin is extended to 3000 GeV.

The reconstructed dilepton invariant mass distribution can be affected by an imperfect lepton momentum measurement. Such effects are nonnegligible and therefore need to be corrected. A bias in the muon momentum reconstruction can occur due to the differences in the tracker misalignment between data and MC as well as the residual magnetic field mismodeling. The momentum scale corrections are applied using the same CMS procedure as performed in previous results described in [10, 26].

5 Background Estimation

The composition of background sources is dependent on the dilepton mass region. The dominant background in the entire mass region are $t\bar{t}$ processes, however DY production of $\tau^+\tau^-$ pairs is dominant below the Z peak. QCD multijet background is relatively dominant at low masses (below 60 GeV).

The main backgrounds are estimated using a control data sample. For the $t\bar{t}$, single top (tW, $\bar{t}$W), DY production of $\tau^+\tau^-$ pairs and diboson (WW), the backgrounds are estimated from an $e\mu$ data sample. These final states contain electron-muon pairs at twice the rate of dimuon and therefore the dimuon can be scaled by the $e\mu$ events properly after accounting for the detector acceptance and efficiency. This method can reduce the systematic uncertainty due to the imperfect theoretical knowledge of the cross sections of the SM processes.

QCD multijet background and W+jets background contain at least one misidentification of the muon and hence the backgrounds are estimated using the "misidentification rate" method described in [27]. In this method the misidentification rate is defined as the fraction of the loosely isolated muons which pass the final isolation requirement. The loosely isolated muons are collected by no isolation requirement after applying the muon identification creteria described above. The misidentification rate is measured as a function of p_T in the barrel and endcap subdetectors separately. For this measurement a data sample selected with the single muon trigger is used, consisting of muon candidates that satisfy the loose isolation requirement. The contributions from a single muon such as DY and $t\bar{t}$ are contaminated in the sample and they are suppressed with an evaluation using a template fit. The misidentification rate is then applied to events selected with criteria to collect loosely isolated leptons after properly subtracting the contributions of real dilepton events.

Other diboson backgrounds (WZ and ZZ) are evaluated using MC simulation. The MC simulations are normalised using the integrated luminosity and higher order theoretical cross sections. The photon-initiated production of muon pairs is estimated with the FEWZ 3.1 program [28, 29], using the MRST2004qed photon PDF and the PYTHIA8 is alternatively used as a

cross-check. The effects are negligibly small for the entire mass range [30].

The expected shapes of dimuon yields from data and signal and backgrounds are shown in Fig. 1 as a function of dimuon invariant mass.

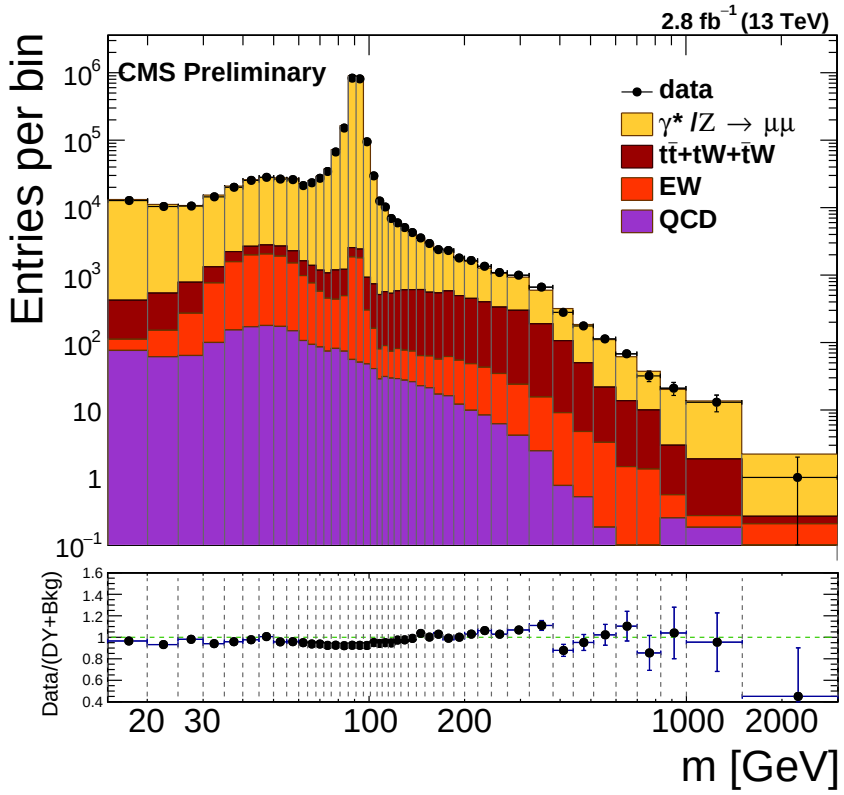

Figure 1: The observed dimuon invariant mass spectra within the detector acceptance. The EW contributions indicate the DY $\rightarrow \tau^+\tau^-$, diboson, and W+jets productions. Error bars are statistical only.

6 Corrections

In this section, we describe how to apply corrections after extracting signal candidates obtained by background subtraction. To the signal candidates from the data sample, we apply correction for the detector resolution effect using unfolding technique. Then acceptance and efficiency are estimated using signal MC samples and apply to the events. Third step of correction is to take into account the difference between data and MC on the selection efficiency and therefore the scale factor of the efficiency is applied. Finally the FSR correction is applied using the dressed lepton definition and unfolding technique. The details of correction procedures are discussed as follows.

6.1 Detector Resolution Effects

The effect of detector resolution leads to a migration of events from bin i of the true distribution to bin k of the reconstructed mass distribution. In order to compare the measured dilepton distributions with theory, this effect of migration is corrected through unfolding. The procedure uses the yield distribution determined from simulation by mapping it onto the measured

one to obtain the true distribution. The unfolding procedure for this analysis is similar to the previous measurement [10] and described as below.

The unfolding response matrix T_{ik}, which gives the fraction of events from bin i of the true (post-FSR) distribution that end up reconstructed in bin k, is calculated from the DY MC simulation.

$$N_{obs,i} = \sum_k T_{ik} N_{true,k}. \tag{2}$$

The matrix is nearly diagonal as more than 90% of the events are on the diagonal. Off-diagonal elements are located adjacent to the main diagonal and the response matrix is invertible. The unfolding procedure using the response matrix is performed using the iterative D'Agostini method [31]. The validity of the unfolding method is tested on the pure signal MC. The effect of unfolding on the differential cross section is largest in the Z peak region (up to 30%) because of the narrow mass bin width used in this measurement.

6.2 Acceptance and Efficiency

The acceptance is defined as the fraction of simulated signal events with both leptons passing the nominal p_{T} and η requirements of the analysis: $p_{\mathrm{T}} > 22(10)$ GeV for leading (subleading) muons with $|\eta| < 2.4$. It is calculated with respect to the full phase space and obtained using the MC sample. The efficiency is defined as the fraction of events in the DY simulated sample that are inside the acceptance and pass the full event selection. The following equation shows the definition of the acceptance and efficiency:

$$A \cdot \varepsilon = \frac{N^A}{N^{gen}} \cdot \frac{N^\varepsilon}{N^A} \tag{3}$$

where N^{gen} is the total number of generated signal events given the invariant mass bins without any acceptance requirements, N^A is the number of events passing the acceptance criteria, and N^ε is the number of events passing the full event selection requirement. Fig. 2 shows the results as a function of the dilepton invariant mass.

6.3 Efficiency Correction

The corrections for lepton reconstruction, identification, isolation, and trigger efficiencies are necessary to account for differences between data and MC events. The corrections are obtained from data-driven technique using $\mathrm{Z} \to l^+l^-$ events where one lepton satisfied the tight selection requirements and the required selection was probed on the other lepton (tag-and-probe method) [32].

The measured efficiency using the tag-and-probe method is parametrised by lepton p_{T} and η and then factorised into the reconstruction, identification, and isolation efficiencies and the event trigger efficiency that accounts for the single lepton trigger requirement. The total event selection efficiency factorised is

$$\varepsilon_{\mathrm{event}} = \varepsilon_{l_1} \cdot \varepsilon_{l_2} \cdot \varepsilon_{\mathrm{event,trig}} \tag{4}$$

where ε_l is the single lepton efficiency and $\varepsilon_{event,trig}$ is the trigger efficiency on the event.

The single muon efficiency is defined as follows:

$$\varepsilon_\mu = \varepsilon_{\mathrm{track}} \cdot \varepsilon_{\mathrm{reco+id}} \cdot \varepsilon_{\mathrm{iso}}. \tag{5}$$

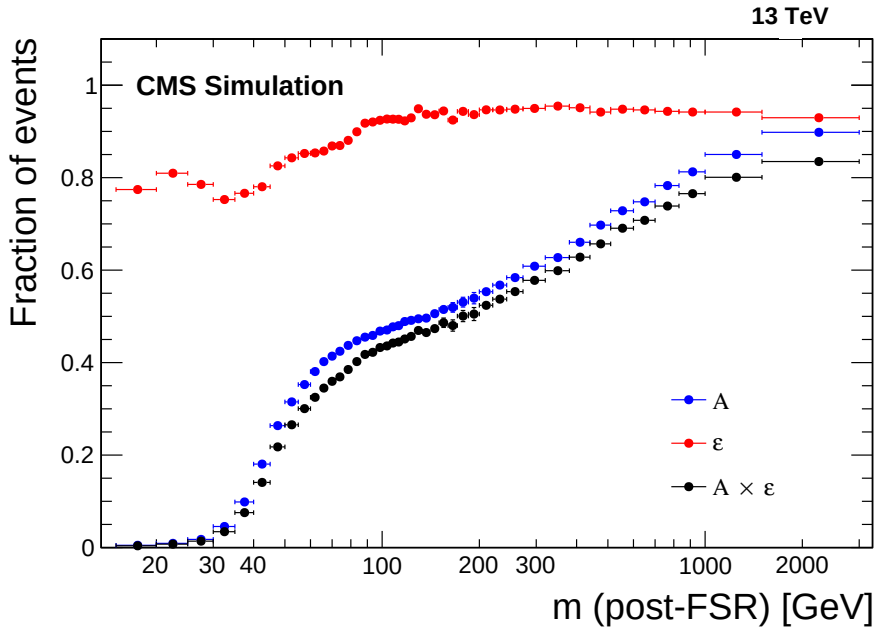

Figure 2: The DY acceptance (A), efficiency (ε) and their product per invariant mass bin.

For the trigger efficiency is defined as follows:

$$\varepsilon_{\text{event,trig}} = \varepsilon_{l_1,\text{trig}} + \varepsilon_{l_2,\text{trig}} - \varepsilon_{l_1,\text{trig}} \cdot \varepsilon_{l_2,\text{trig}}. \tag{6}$$

The scale factor between data and MC is determined by $\varepsilon_{\text{data}}(\text{event})/\varepsilon_{\text{MC}}(\text{event})$. The scale factors are measured to be in the range of 0.92–0.97 and the range is dependent on the data taking period. They are applied to MC simulations to take into account the difference.

6.4 Final State QED Radiation Effects

The effect of photon radiation from the final-state leptons shifts the measured invariant mass of the dilepton pair to lower values, which significantly effects the distribution below the Z peak. A correction for FSR is performed in order to compare the results to theoretical predictions and facilitate the combination with other channels. For the correction, the concept of the "dressed" lepton is used. The dressed lepton four-momentum is defined as

$$p_l^{\text{dressed}} = p_l^{\text{post-FSR}} + \Sigma p_\gamma, \tag{7}$$

where the four momenta of all the simulated photons originating from leptons are summed within a cone of $\Delta R < 0.1$.

The FSR correction is estimated separately from the detector resolution correction by means of the similar unfolding technique. The response matrix is produced using the dressed dilepton and post-FSR dilepton. The correction to the cross section from the post-FSR to the dressed lepton is found to be in the range 0.92–1.28 and the affect is dominated at below the Z peak.

7 Systematic Uncertainties

The dominant systematic uncertainties are different according to the mass ranges. The efficiency scale factor is the dominant source of systematic uncertainty at and below the Z-peak regions. This uncertainty includes muon reconstruction, identification, isolation, and trigger selection. A variety of possible systematic sources in the efficiency scale factor has been investigated and can listed as:

- statistical uncertainty associated with the tag-and-probe procedure
- binning in single muon p_{T} and η
- shape hypothesis of signal and background in the fit model
- other minor sources: the number of mass bin, mass range, p_{T} criteria.

Uncertainties for all sources are evaluated separately and are combined in quadrature sum. The total systematic uncertainty for the efficiency scale factor is found to be 1.0–3.3% below the Z-peak region, 0.6–1.0% in the Z-peak region, and 1.0–2.5% above the Z-peak region.

The detector resolution effect, including the muon momentum scale correction, is dominant at and above the Z-peak regions. Both MC and data are smeared by varying the muon momentum scale within its uncertainty. The difference between the central value and the smeared result on the cross section is assigned as a systematic uncertainty in each mass bin. In addition, two other main sources for systematic uncertainties in the detector resolution unfolding are considered:

- the statistical uncertainty on the response matrix due to the finite size of the MC sample, and
- the systematic uncertainty on the response matrix from deficiencies in the MC modeling by comparing two different MC generators (between MADGRAPH5_AMC@NLO and POWHEG).

Systematic uncertainties for the background estimation using data samples are correlated with statistics and therefore the statistical uncertainty of the control region drives the systematic uncertainties in the high mass regions (above 200 GeV). The Poissonian statistical uncertainty of the estimated backgrounds is a main source in the calculation of systematic uncertainty. Backgrounds estimated using data sample consider the difference between the predictions from data and MC simulation. In the cases where the backgrounds are estimated from MC simulation, the uncertainty of the cross section is included as a systematic uncertainty.

Systematic uncertainty on the acceptance is dominated by the theoretical uncertainty. The theoretical uncertainty is mainly caused by imperfect knowledge of the non-perturbative PDFs. The PDF uncertainties are estimated using the FEWZ program with NNLO. In the estimation FEWZ uses a reweight technique with the LHAGLUE interface to the PDF library LHAPDF as described in [33–35] The FEWZ calculation also includes high order (NLO) electroweak (EW) correction and FSR correction using the dressed lepton definition in order to take into account the effects. EW corrections are relatively small to compare to FSR corrections. The DY cross section has a dependence on the strong coupling constant, α_s. The uncertainty is evaluated by varying α_s between 0.117 and 0.119 in the calculation of the DY cross section using FEWZ with NNLO PDF, where the central value of α_s is 0.118.

The systematic uncertainty due to the model-dependent FSR simulation is evaluated using the comparison between two different generator. The FSR simulation in the DY signal MC is performed with PYTHIA8 and we compare the modeling to the PHOTOS [36, 37] generator. Difference on the cross section after FSR correction using dressed lepton and unfolding procedure

between the PYTHIA8 and the PHOTOS generators are assigned as systematic uncertainties.

The uncertainty on the luminosity measurement is obtained with 2.7% that is based on pixel cluster counting from the silicon pixel detector. More details are described in [38]. Fig. 3 shows the results of systematic uncertainties obtained in each mass bin.

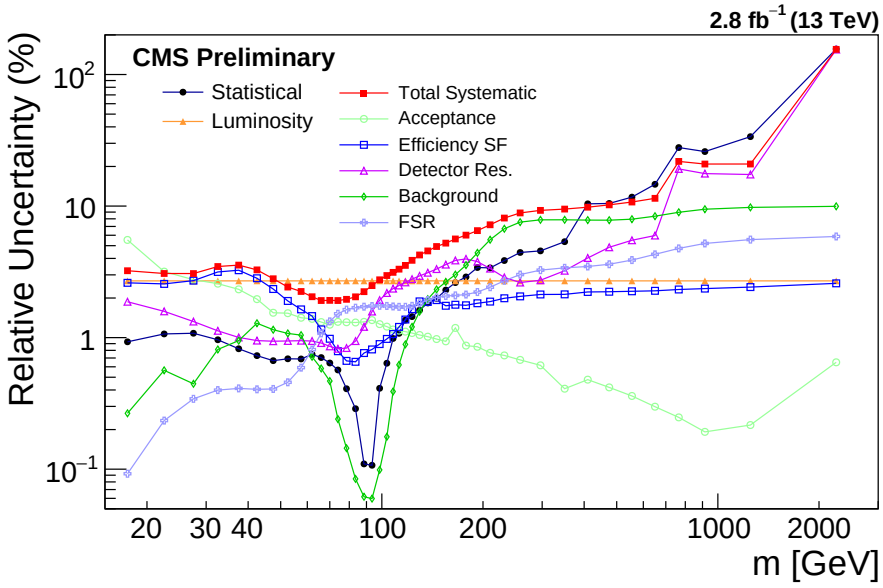

Figure 3: Summary of the systematic uncertainties for $d\sigma/dm$ measurement. The "Total Systematic" is a quadratic sum of all systematic uncertainty sources except for the Acc.+PDF.

8 Results

The DY differential cross section in the full phase space is measured after full corrections described in the previous sections. The results are presented in Fig. 4 as a function of dimuon invariant mass. They are compared to the NNLO theoretical predictions which are calculated using FEWZ 3.1 with NNPDF3.0 and NLO EW correction as well as MADGRAPH5_AMC@NLO predictions with NNPDF3.0 (NLO). As shown in the figure, the DY differential cross section with full corrections covers the range of 15 to 3000 GeV and are divided by the invariant mass bin widths. The ratio between data and theoretical prediction is shown in the middle and bottom plots. Differences between FEWZ and MADGRAPH5_AMC@NLO are shown in the plots. The results of the measurement are in good agreement with both theoretical predictions within uncertainties. The band with red colour on the middle and bottom plots in the figure denotes total uncertainty which is the combination of statistical, systematical, theoretical, and luminosity uncertainties in quadrature. The band with purple colour denotes the statistical uncertainty only.

In additional to the fully corrected DY differential cross section measurement, the result of the fiducial cross section, within the detector acceptance and without FSR correction, is produced. Figure 5 shows the results compared to the NLO predictions by MADGRAPH5_AMC@NLO. The results are in good agreement with the theoretical prediction.

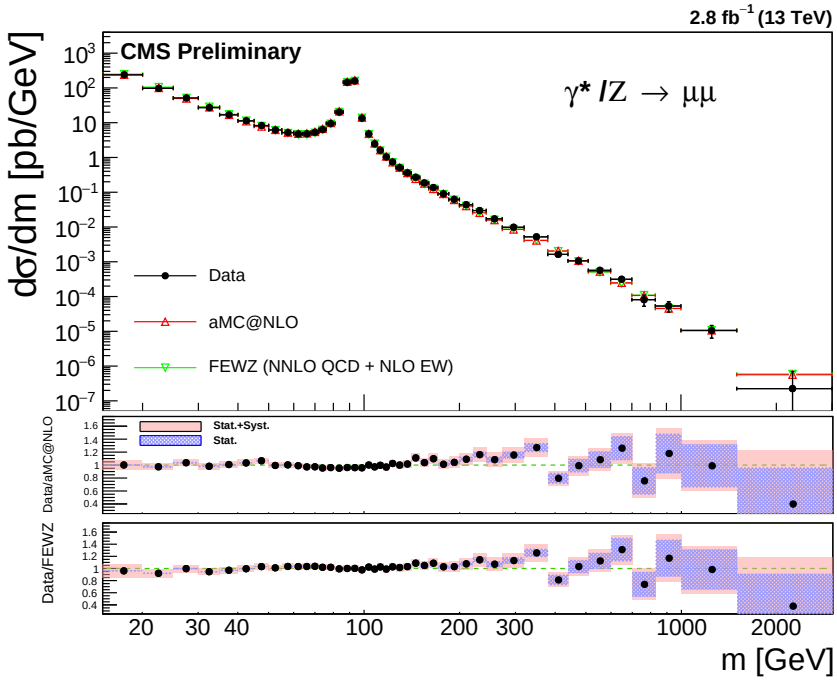

Figure 4: Result of the DY differential cross section measurement for full phase space with FSR correction as a function of dimuon invariant mass compared to the NNLO theoretical prediction of FEWZ (red) and the NLO prediction of MADGRAPH5_AMC@NLO (green). Both NNPDF3.0 PDF set is used for the theoretical calculation. In the middle and bottom plots, the band with red colour denotes total uncertainty which is the combination of statistical, systematical, theoretical, and luminosity uncertainties. The band with purple colour denotes the statistical uncertainty only.

9 Summary

In summary, this note presented results of the measurement of the Drell-Yan differential cross section $d\sigma/dm$ in the dimuon channel in the mass range $15 < m < 3000$ GeV in proton-proton collisions at $\sqrt{s} = 13$ TeV. The measurement is based on the dataset corresponding to an integrated luminosity of 2.8 fb^{-1}. The measurement is corrected for detector resolution correction resulting in event migration between mass bins, efficiency caused by the difference between data and MC simulation, acceptance to take into account the coverage of CMS detector, and FSR effects pronounced mostly below the Z peak. The results are in good agreement with the SM theoretical predictions at NNLO predictions calculated with FEWZ and NLO predictions calculated with MADGRAPH5_AMC@NLO.

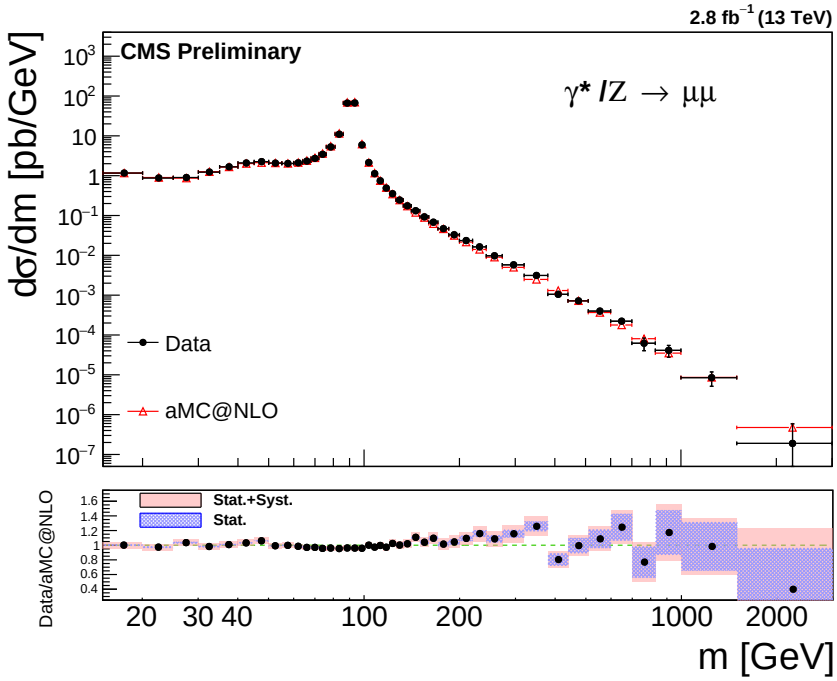

Figure 5: Comparison between the experimental results for fiducial cross section without FSR correction and the NLO theoretical prediction using MADGRAPH5_AMC@NLO. On the bottom plot, the band with red colour denotes total uncertainty which is the combination of statistical, systematical, and luminosity uncertainty. The band with purple colour denotes the statistical uncertainty only.

References

[1] R. Hamberg, W. L. van Neerven, and T. Matsuura, "A complete calculation of the order α_s^2 correction to the Drell–Yan K-factor", *Nucl. Phys. B* **359** (1991) 343, doi:10.1016/0550-3213(91)90064-5. Erratum-ibid. B644 (2002) 403-404.

[2] S. Catani et al., "Vector Boson Production at Hadron Colliders: A Fully Exclusive QCD Calculation at Next-to-Next-to-Leading Order", *Phys. Rev. Lett.* **103** (2009) 082001, doi:10.1103/PhysRevLett.103.082001, arXiv:0903.2120.

[3] S. Catani and M. Grazzini, "Next-to-Next-to-Leading-Order Subtraction Formalism in Hadron Collisions and its Application to Higgs-Boson Production at the Large Hadron Collider", *Phys. Rev. Lett.* **98** (2007) 222002, doi:10.1103/PhysRevLett.98.222002, arXiv:hep-ph/0703012.

[4] K. Melnikov and F. Petriello, "Electroweak gauge boson production at hadron colliders through O(α_s^2)", *Phys. Rev. D* **74** (2006) 114017, doi:10.1103/PhysRevD.74.114017, arXiv:hep-ph/0609070.

[5] F. Goertz, A. Katz, M. Son, and A. Urbano, "Precision Drell-Yan Measurements at the LHC and Implications for the for the Diphoton Excess", arXiv:1602.04801.

[6] ATLAS Collaboration, "Measurement of the high-mass Drell–Yan differential cross-section in pp collisions at $\sqrt{s} = 7$ TeV with the ATLAS detector", *Phys. Lett. B* **725** (2013) 223, doi:10.1016/j.physletb.2013.07.049, arXiv:1305.4192.

[7] ATLAS Collaboration, "Measurement of the low-mass Drell–Yan differential cross section at $\sqrt{s} = 7$ TeV using the ATLAS detector", *JHEP* **06** (2014) 112, doi:10.1007/JHEP06(2014)112, arXiv:1404.1212.

[8] CMS Collaboration, "Measurement of the Drell–Yan Cross Section in pp Collisions at $\sqrt{s} = 7$ TeV", *JHEP* **10** (2011) 007, doi:10.1007/JHEP10(2011)007, arXiv:1108.0566.

[9] CMS Collaboration, "Measurement of the differential and double-differential Drell–Yan cross sections in proton-proton collisions at $\sqrt{s} = 7$ TeV", *JHEP* **12** (2013) 030, doi:10.1007/JHEP12(2013)030.

[10] CMS Collaboration, "Measurement of differential and double-differential Drell–Yan cross sections in proton-proton collisions at $\sqrt{s} = 8$ TeV", *Eur. Phys. J.* **C 75** (2015) 147, doi:10.1140/epjc/s10052-015-3364-2.

[11] CMS Collaboration, "Performance of electron reconstruction and selection with the CMS detector in proton-proton collisions at $\sqrt{s} = 8$ TeV", *JINST* **10** (2015) P06005, doi:10.1088/1748-0221/10/06/P06005, arXiv:1502.02701.

[12] CMS Collaboration, "Performance of CMS muon reconstruction in pp collision events at $\sqrt{s} = 7$ TeV", *JINST* **7** (2012) P10002, doi:10.1088/1748-0221/7/10/P10002, arXiv:1206.4071.

[13] CMS Collaboration, "The CMS experiment at the CERN LHC", *JINST* **3** (2008) S08004, doi:10.1088/1748-0221/3/08/S08004.

[14] J. Alwall et al., "The automated computation of tree-level and next-to-leading order differential cross sections, and their matching to parton shower simulations", *JHEP* **07** (2014) 079, doi:10.1007/JHEP07(2014)079, arXiv:1405.0301.

[15] R. D. Ball et al., "A first unbiased global NLO determination of parton distributions and their uncertainties", *Nucl. Phys. B* **838** (2010) 136.

[16] NNPDF Collaboration, "Parton distributions for the LHC Run II", *JHEP* **04** (2015) 040, doi:10.1007/JHEP04(2015)040, arXiv:1410.8849.

[17] R. Frederix and S. Frixione, "Merging meets matching in MC@NLO", *JHEP* **1212** (2012) 061, doi:10.1007/JHEP12(2012)061, arXiv:1209.6215.

[18] P. Nason, "A New Method for Combining NLO QCD with Shower Monte Carlo Algorithms", *JHEP* **11** (2004) 040, doi:10.1088/1126-6708/2004/11/040.

[19] S. Frixione, P. Nason, C. Oleari, "Matching NLO QCD computations with parton shower simulations: the POWHEG method", *JHEP* **11** (2007) 070, doi:10.1088/1126-6708/2007/11/070.

[20] S. Alioli, P. Nason, C. Oleari, and E. Re, "A General Framework for Implementing NLO Calculations in Shower Monte Carlo Programs: the POWHEG BOX", *JHEP* **06** (2010) 043, doi:10.1007/JHEP06(2010)043.

[21] S. Alioli, P. Nason, C. Oleari, and E. Re, "NLO Vector Boson Production Matched with Shower in POWHEG", *JHEP* **07** (2008) 060, doi:10.1088/1126-6708/2008/07/060.

[22] T. Sjstrand et al., "An Introduction to PYTHIA 8.2", *Comput. Phys. Commun.* **191** (2015) 159–177, doi:10.1016/j.cpc.2015.01.024, arXiv:1410.3012.

[23] CMS Collaboration, "Event generator tunes obtained from underlying event and multiparton scattering measurements", *Eur. Phys. J. C* **76** (2016), no. 3, 155, doi:10.1140/epjc/s10052-016-3988-x, arXiv:1512.00815.

[24] GEANT4 Collaboration, "GEANT4 – a simulation toolkit", *Nucl. Instrum. Meth. A* **506** (2003) 250, doi:10.1016/S0168-9002(03)01368-8.

[25] CMS Collaboration, "Muon Reconstruction and Identification Improvements for Run-2 and First Results with 2015 Run Data", Technical Report CMS-DP-15-015, CERN, Geneva, 2015.

[26] A. Bodek et al., "Extracting muon momentum scale corrections for hadron collider experiments", *Eur. Phys. J. C* **72** (2012) 2194, doi:10.1140/epjc/s10052-012-2194-8, arXiv:1208.3710.

[27] CMS Collaboration, "Search for physics beyond the standard model in dilepton mass spectra in proton-proton collisions at $\sqrt{s} = 8$ TeV", *JHEP* **04** (2015) 025, doi:10.1007/JHEP04(2015)025, arXiv:1412.6302.

[28] R. Gavin, Y. Li, F. Petriello, and S. Quackenbush, "FEWZ 2.0: A code for hadronic Z production at next-to-next-to-leading order", *Comput. Phys. Commun.* **182** (2011) 2388, doi:10.1016/j.cpc.2011.06.008, arXiv:1011.3540.

[29] Y. Li and F. Petriello, "Combining QCD and electroweak corrections to dilepton production in FEWZ", *Phys. Rev. D* **86** (2012) 094034, doi:10.1103/PhysRevD.86.094034.

[30] D. Bourilkov, "Photon-induced Background for Dilepton Searches and Measurements in pp Collisions at 13 TeV", arXiv:1606.00523.

[31] G. D'Agostini, "A multidimensional unfolding method based on Bayes' theorem", *Nucl. Instrum. Meth. A* **362** (1995) 487, doi:10.1016/0168-9002(95)00274-X.

[32] CMS Collaboration, "Measurement of the inclusive W and Z production cross sections in pp collisions at $\sqrt{s} = 7$ TeV with the CMS experiment", *JHEP* **10** (2011) 132, doi:10.1007/JHEP10(2011)132, arXiv:1107.4789.

[33] M. R. Whalley, D. Bourilkov, and R. C. Group, "The Les Houches accord PDFs (LHAPDF) and LHAGLUE", in *HERA and the LHC: A Workshop on the implications of HERA for LHC physics. Proceedings, Part B*. 2005. arXiv:hep-ph/0508110.

[34] D. Bourilkov, R. C. Group, and M. R. Whalley, "LHAPDF: PDF use from the Tevatron to the LHC", in *TeV4LHC Workshop - 4th meeting Batavia, Illinois, October 20-22, 2005*. 2006. arXiv:hep-ph/0605240.

[35] A. Buckley et al., "LHAPDF6: parton density access in the LHC precision era", *Eur. Phys. J.* **C75** (2015) 132, doi:10.1140/epjc/s10052-015-3318-8, arXiv:1412.7420.

[36] E. Barberio, B. van Eijk, and Z. Was, "PHOTOS - a universal Monte Carlo for QED radiative corrections in decays", *Comput. Phys. Commun.* **66** (1991) 115, doi:10.1016/0010-4655(91)90012-A.

[37] E. Barberio and Z. Was, "PHOTOS - a universal Monte Carlo for QED radiative corrections: version 2.0", *Comput. Phys. Commun.* **79** (1994) 291, doi:10.1016/0010-4655(94)90074-4.

[38] CMS Collaboration, "CMS Luminosity Measurement for the 2015 Data Taking Period", CMS Physics Analysis Summary CMS-PAS-LUM-15-001, 2015.